RICE UNIVERSITY

The transition from a TEM-like mode to a plasmonic mode in finite-width THz parallel-plate waveguides

by

Jingbo Liu

A THESIS SUBMITTED
IN PARTIAL FULFILLMENT OF THE
REQUIREMENTS FOR THE DEGREE

Master of Science

APPROVED, THESIS COMMITTEE

Daniel Mittleman, Professor,Chair
Electrical and Computer Engineering

Kevin Kelly, Associate Professor,
Electrical and Computer Engineering

Qianfan Xu, Assistant Professor
Electrical and Computer Engineering

HOUSTON, TEXAS
February 2011

Abstract

The transition from a TEM-like mode to a plasmonic mode in finite-width THz parallel-plate waveguides

by

Jingbo Liu

By the near-field measurement of the electric field distribution inside the finite width THz parallel plate waveguide, we find the transition from conventional diffractive TEM-like mode to plasmonic mode. This mode transition depends on the geometry of the waveguide. The measurement is conducted on THz-TDS system with scattering probe-technique. We present the simulation which agrees with our experimental data

Acknowledgments

I would like to thank my advisor, Dr. Daniel Mittleman, for guidance and strong support. I would like to thank Dr. Rajind Mendis, for working with me closely until I can work independently and for his good suggestions in this project. Also I owe to my group members Hui Zhan, Victoria Astley, for their useful discussions and contributions to this work. Last I would like to thank my Chinese friends here at Rice and my loving parents.

Contents

Abstract ii

Acknowledgements iii

Contents iv

1. INTRODUCTION 1

2. Experimental Setup and Method 2

3. Experimental results 6

4. Numerical simulations 11

5. Conclusions 20

REFERENCES 21

1. Introduction

Parallel plate waveguides (PPWGs) have been intensively studied in the last decade with terahertz radiation. The fundamental propagation mode of the PPWG is TEM mode, which supports dispersionless propagation with low loss and no cut-off.[1] [2] [3] [4] This waveguide is therefore well suited for the transport of broadband terahertz pulses, and has been exploited for spectroscopic measurements,[5] [6] [7] [8] [9]imaging, [10]and sensing.[11] [12] [13]Recently the finite-width PPWG was used to focus both terahertz [14] and infrared waves [15] into extreme subwavelength areas, by adiabatic tapering of both the waveguide width and the plate separation. In this case, the efficient confinement from the two air sides is somewhat surprising, and opens up new applications such as high-resolution near-field THz imaging and THz wave coupling into subwavelength-sized devices. In order to optimize this extreme field confinement or to develop novel THz devices such as mode converters[16], a detailed understanding of the field distribution inside the finite-width waveguide is required.

In section 2, we discuss our experimental set-up and detection approach, which is based on scattering probe imaging,[17] a technique similar to apertureless near-field optical microscopy (ANSOM). In section 3, we show the results from the sub-wavelength-resolved measurements of the cross-section field distribution inside a finite-width THz PPWG. We observe that there is a transition of propagating mode from the conventional TEM-like mode (at the longest wavelengths) to a mode more characteristic of a plasmonic confinement mechanism (at shorter wavelengths). The frequency in which this kind of mode transitions occur depends on the waveguide geometry. In section 4, we show the numerical simulation, conducted on COMSOL MultiPhysics software and MATLAB, which support our experimental results. We give a theoretical explaination

for the waveguide geometry dependence and wavelength dependence of the mode transition frequency.

2. Experimental Setup and Method

Our experiment setup consists of THz transmitter and receiver (fibre coupled photoconductive antennas, Fig1(a)), finite-width parallel plate waveguide, piezo-transducor, lock-in amplifier, and metal wire scatterer. The waveguide has two Aluminum cubic plates, with width and thickness of 1cm, and length of 25cm. Each plate has one face (25cm x 1cm face) highly lapped to ~10μm. The plates are mounted so that the polished faces are parallel to each other with a variable separation. The THz wave polarized normal to the polished surfaces is focused by silicon lense into a beam waist of ~1cm, exciting to the input face of the waveguide. A pinhole of 1cm diameter is used to control the exciting area at the waveguide input facet, shown in Fig 1 b). The TEM-like waveguide mode can be effectively excited in this way. [1]

For the detection of the signal inside the waveguide we employed scattering probe imaging[17], a technique similar to apertureless near-field optical microscopy (ANSOM). We mounted a probe, usually the commercialized tungsten needle or berrylium-copper needle, on the piezo-tranducor. As in ANSOM, the position of the scatterer is modulated at a few hundred Hz using a piezoelectric mounting, so that the signal reaching the detector from the scatterer can be extracted via lock-in detection. We have developed this scattering-type detection method for characterization and imaging of THz fields with subwavelength resolution.[17][14] Unlike in conventional ANSOM, the detection is phase-sensitive, which has significant advantages. For example, even if the field to be measured is spatially uniform, the differential detection still generates a non-zero signal

due to the phase difference induced by modulation of the position of the scatterer relative to the (fixed) THz detector.[17]

The probe of the scattering-probe technique was selected carefully to meet the measurement requirements. In our near-field measurement, the ideal probe needs to be inserted into the narrow slit between the two plates, not influencing the field distribution too much, and preserving the bandwidth of the signal as broad as possible. The probe consists of two parts: the dielectric (wood) holder and the tiny metal scatterer. The wooden holder is a flat wedge of tickness 300 micron. Since wood is relatively invisible in THz range, the wooden holder has very little influence on the field inside the waveguide. A tiny sub-wavelength metal scatterer, stick to tip of the wooden holder, help scatter the signal out to the receiver. (Fig 1c). To meet the bandwith requirement we chose the scatterers of simple shape (spherical or cylindrical) and appropriate size. Table 1 lists the scatterer we have tested. Figure 1 d shows the signals of a few scatterers in Table 1. Balaching the SNR, bandwidth, and spatial resolution, finally we chose the Al wire scatterer of length 2mm and diameter 200 micron as our final scatterer.

Scatterer	Diameter / μm	Length / mm
Stainless steel /Aluminum	50, 100, 200	1, 2, 3
Silver coated glass ball	10, 20, 50	

Table 1: The scatterer testing list

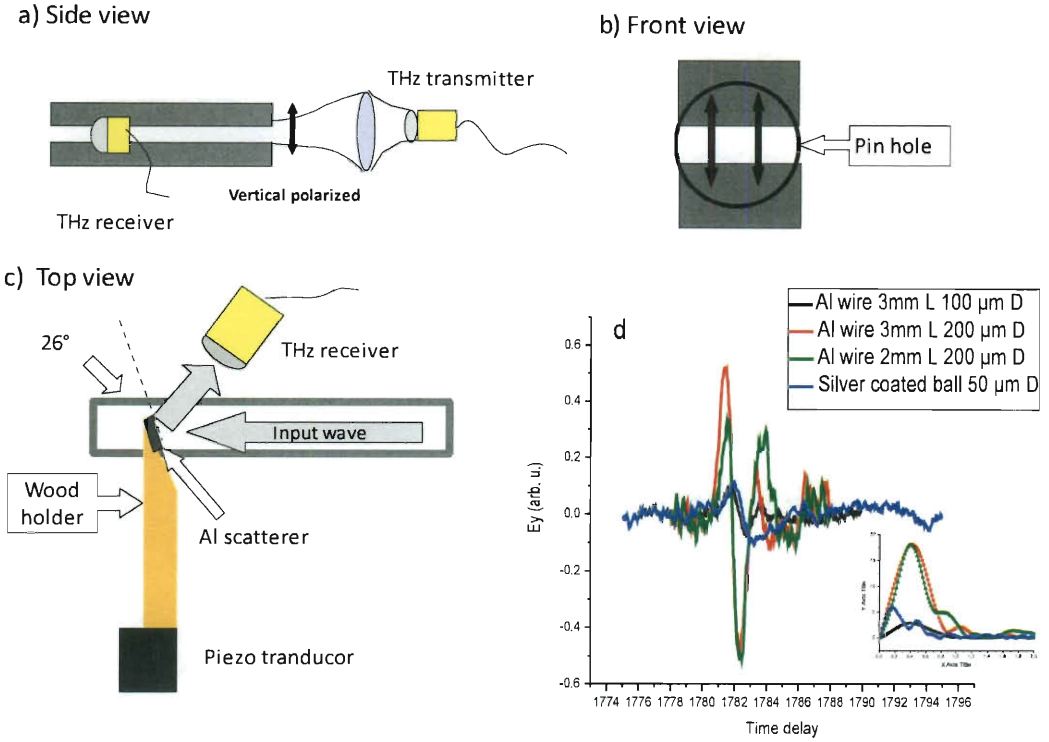

Figure 1 Experiment set-up: a) The side view of the set-up, the wave is polarized perpendicular to the plate b) The front view of the input facet, black circle is the boundary of pin hole c) The scheme of the ANSOM technique in top view d) The test signals for different scatterers, the inset shows the spectrum for each signal.

The metal wire scatterer is oriented 26° from noraml to the propagating direction, see Fig 1 c), oscillating at 180Hz frequency with ~1μm amplitude. The guided wave encounters the scatterer 22.5cm downstream from the input facet and be scattered toward the receiver which is fixed in the specular direction ~1cm away from the wire. The scattering probe can be translated into and out of the waveguide, along a line perpendicular to the waveguide axis and centered between the two plates. Time-domain waveforms are measured using a conventional optical delay line.

Fig. 2 shows typical waveforms detected when the scattering probe is inside the waveguide, at the waveguide edge, and outside the waveguide, representing subwavelength-resolved measurements of the local THz field at these locations. The bottom left inset illustrates a cross-section of the waveguide with colored dots indicating the measurement locations. The bottom right inset shows the spectra for the three signals, all of which show spectral bandwidth comparable to that of the input pulse. This indicates that the subwavelength scatterer is not imposing any significant spectral distortion or filtering on the measured signals.[18]

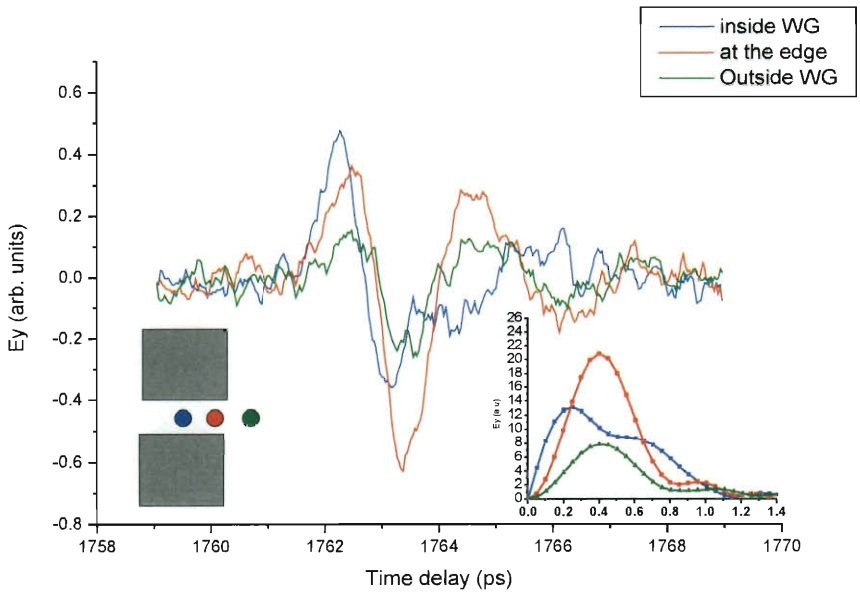

Figure 2 The sigals detected by scattering probe technique at different location. The right bottom inset is the spectrum of the signals and the left bottom inset is the location of the detections.

3 . Experimental results

We use the scattering probe technique to characterize the frequency-dependent field distribution inside the waveguide. Since the PPWG and the input excitation spot are both symmetric with respect to the plane parallel to the propagation direction and perpendicular to the plate surfaces, we only need to scan the probe through one half of the waveguide, from this central plane out. Fig 3 (a) and (c) show the signal spatial distribution at different frequency,0.15 THz, 0.40 THz and 0.55 THz, for plate separation b of 1mm and 2mm. The PPWG plate edges are located at x = ±5mm (the plate width is 1cm). Fig3 (b) and (d) show the signal spectrum at different locations relative to the middle where x = 0mm. Fig3(a), the TEM-like mode pattern shows up both in 0.15 THz and 0.40 THz, with 0.15THz signals more diffractive. The diffraction of the signal is stronger if it is closer to the edge or if it is in the longer wavelength. So the diffractive TEM-like mode shows a single peak in the middle of the waveguide, as in 0.15 THz. The 0.55 THz signal spatial distribution turns into plasmonic mode-like, which has stronger edge field.[19] In Fig 3(c), we observe the same mode transition, except the plasmonic mode starts showing up in 0.40 THz. In Fig 3(b) and (d) we indentify this mode transition frequency clearly in the spectrum. Fig 3(b) shows the field peak inside waveguide for the frequencies less than ~ 0.42THz and field peak at the edges of waveguide for the frequencies larger than ~0.42THz. So 0.42THz is identified as the transition frequency. The same applies to figure 3(d) and show 0.23THz as transition frequency.

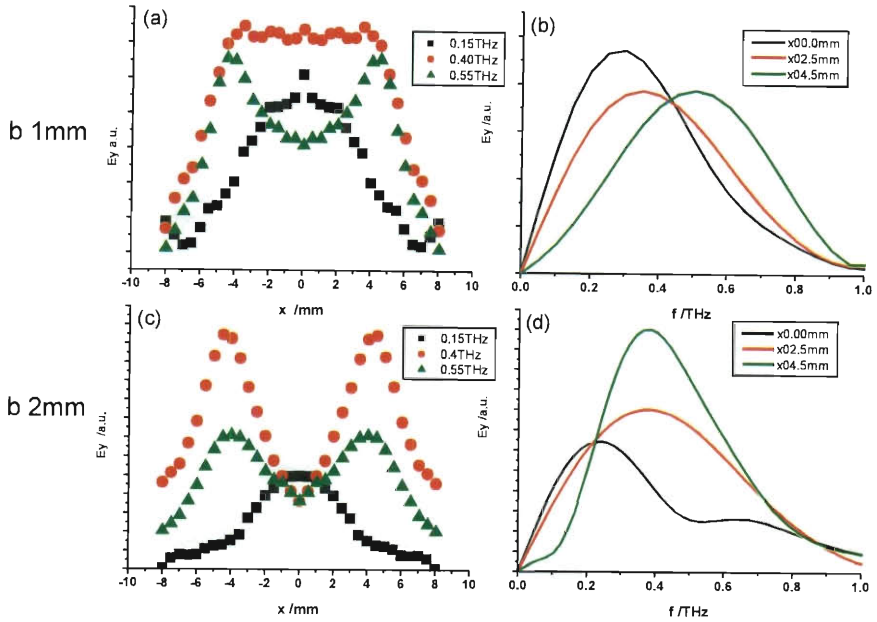

Figure 3 The field spatial and spetra distributions: (a) and (c) are the spatial field distribution for frequency 0.15 THz, 0.4 THz, 0.55 THz. (b) and (d) are the spetra field distribution at location x=0mm (middle), 0.25mm, and 0.45mm (close to the waveguide edge). (a) and (b) have plate separation b =1mm, (c) and (d) have plate spearation 2mm.

In order to emphasize the change of the energy spatial distribution with frequency, we compute the power spectrum of the signal by Fourier transform at each detection location. We then normalize these plots to unity for each frequency to create a two-dimensional plot of the spectral content at each spatial position. The data, shown in Fig. 4 for three different plate separations, are duplicated with respect to the waveguide center at x = 0, for clarity of the display. At low frequencies, we observe that the energy is concentrated in the center of the waveguide, as one would expect for a conventional

TEM-like mode.[20] However, at higher frequencies, there is a rather sharp transition to a distinct mode where the energy is concentrated near the waveguide's edges at x = ±5 mm. This field distribution is strongly reminiscent of the mode of a slot waveguide exhibiting edge plasmons, which has been predicted for optical frequencies[21] [22]and observed in the THz region using near-field measurments of the waveguide output facet. [14] The three panels in Fig. 4 all show qualitatively similar behavior, except that the transition from the low-frequency TEM-like mode to the high-frequency plasmon-like mode occurs at a lower frequency for a larger plate separation.

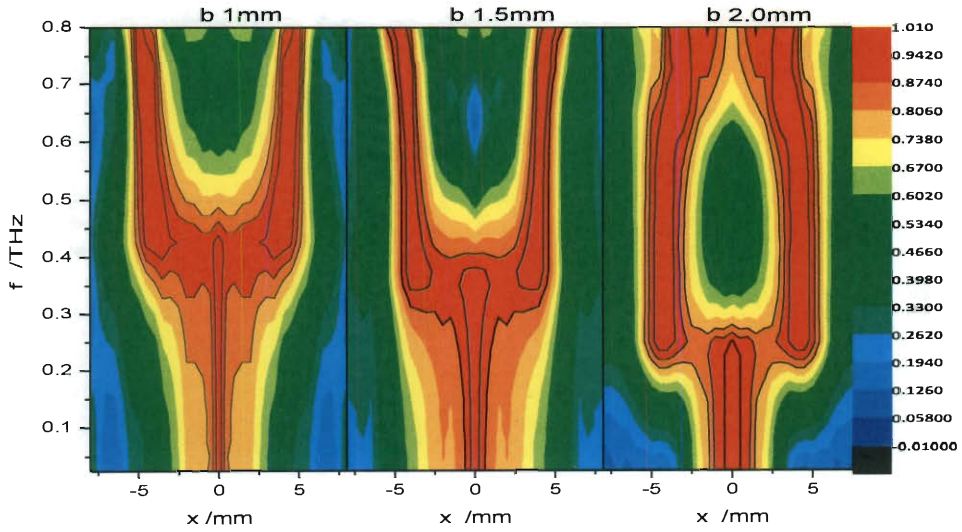

Figure 4 Contour plot of the spetral contents at different locations. The field strength are normalized to 1 at each frequency. The plate spearations for the there panels are 1mm, 1.5mm, 2mm. (from left to right)

We note that these two waveguide modes cannot easily be distinguished using conventional far-field measurements. For metals with very high conductivity (as in the terahertz range), the group velocity and group velocity dispersion of the TEM mode are nearly identical to that of a surface plasmon mode (within a few parts in 10^8). Moreover, strong diffraction at the waveguide's output facet will smooth out any spatial nonuniformities in the far field. The distinction can only be observed with near-field techniques such as the one described here. Nevertheless, for many of the recent applications of finite-width THz PPWGs, the mode distribution inside the waveguide can have a significant impact on the results.

To clarify the mechanism responsible for the spatial mode transition, we can extract a characteristic frequency at which the transition from the TEM-like mode to the plasmon-like mode occurs. This transition frequency is defined as the crossing point between two vertical slices through the two-dimensional plots, at the waveguide center (x = 0) and edge (x = 5 mm) respectively. In Fig. 5 we plot the transition frequencies determined in this manner, for several different plate separations. The transition frequencies are inversely related to plate spearations.

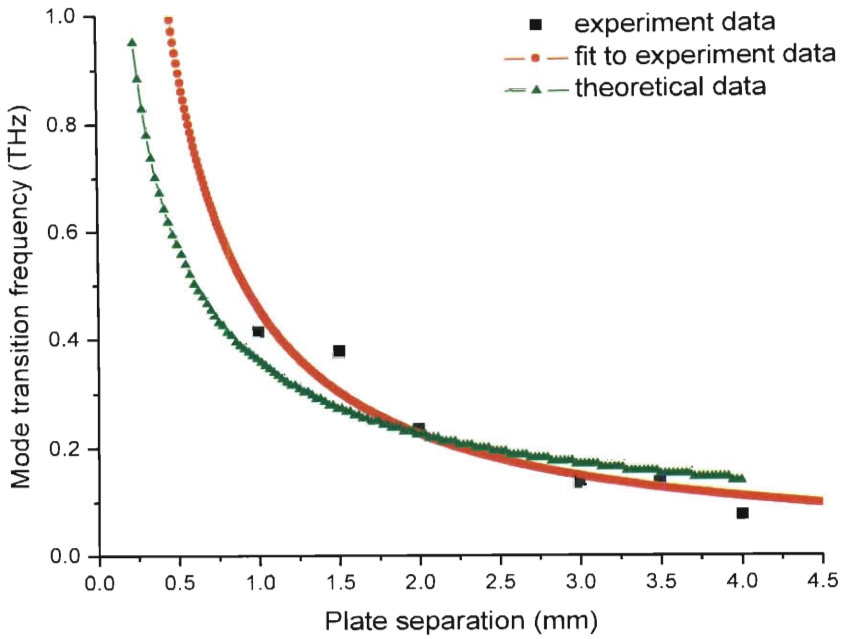

Figure 5 The mode transition frequency vs the plate separation. The black square is the experimental data. The red dot line is the inverse relatio fit to the experimental data by regression method. The green triangle dot line is the calculated data by the simple theoretical model.

We can understand this approximate inverse relationship between the transition frequency and the plate separation as follows. When the plate separation is small, there is strong coupling between the two plates since the separation is much smaller than the decay length of a surface plasmon into air. Thus, the waveguide supports a TEM-like mode.[21] [23] [24] However, when the plate separation is larger, comparable to the plasmon decay length, then the mode transits into two independent surface plasmons. This is analogous to the hybrid mode described by Barlow for infinite plate widths.[25] For finite-width waveguides, this mode shows strong edge enhancements due to the excitation of edge plasmons.[21][14] Therefore, the degree of interaction between the two surface waves at the two plate surfaces strongly influences the experimentally determined

transition frequency.[24] Comparing to our experimental results we employ a simple model to compute this transition frequency for different plate separations, which is discussed in detail in the following section.

4. Numerical simulations

The electric permitivity ε of the metal (Aluminum plates), which changes in magnitude with frequency, is critical for the surface plasmon phenomenon. In THz range, the simple Drude model is usually employed to calculate the permitivity. [26] [27] [28]

However for the surface wave propagations on flat metal sheet, there is a well-known disparity of propagation length or the evanescent field decay length into the dielectric between experiment and theretical calculation with the simple Drude model [26] [27]. There are a few possible reasons for this disparity: one is because of the surface roughness of the flat metal sheet, which changes propagation properties of surface waves on metal sufrace [29][30] Another reason is from the simple Drude model, which is too simplified to describe the multi-crystal Aluminum material. The detailed discussions for this disparity is beyond the scope of this thesis. But we will take it into account by modifying the metal DC conductivity, we call it effective conductivity, in accordance to the experimental propagation length or decay length of the surface wave. The modified effective conductivity is about 1000 times smaller. [26][27] The table bellow is the permitivity for the concerned THz range calculated from the modified and unmodified DC conductivity.

f (Thz)	ε (SI) (modified)	ε (SI) not modified
0.1	-3.59e-10 + 7.29e-08i	-2.87e-07 + 5.69e-05i
0.2	-3.59e-10 + 3.64e-08i	-2.87e-07 + 2.84e-05i
0.3	-3.59e-10 + 2.43e-08i	-2.87e-07 + 1.89e-05i
0.4	-3.59e-10 + 1.82e-08i	-2.87e-07 + 1.42e-05i
0.5	-3.59e-10 + 1.45e-08i	-2.87e-07 + 1.13e-05i
0.6	-3.59e-10 + 1.21e-08i	-2.87e-07 + 9.47e-06i
0.7	-3.59e-10 + 1.04e-08i	-2.87e-07 + 8.12e-06i
0.8	-3.59e-10 + 9.10e-09i	-2.86e-07 + 7.10e-06i
0.9	-3.58e-10 + 8.09e-09i	-2.86e-07 + 6.31e-06i
1	-3.58e-10 + 7.27e-09i	-2.86e-07 + 5.67e-06i
DC σ	22125	3.54E+007

Table 2 The modified and unmodified Aluminum permitivity in THz range

We conduct the numerical simulations on COMSOL multiphysics software, a software based on FEM solution of partial differential equations. We employ the "3D boundary mode analysis application mode" (Hybrid-Mode waves), the most used way, to analyze the waveguide mode. Because our waveguide has finite width and has two sides open to the air, it can not support pure TE or TM mode, but the hybrid-TEM mode. [20] So the application mode we used is appropriate to simulate the waveguide mode with predictable distinctions.

We review this 3D boundary mode analysis application mode briefly. This mode describes the 3D waves as

$$H(x,y,z,t) = H(r_t)\exp(j(\omega t + \beta (n \cdot r))) \qquad (1)$$
$$E(x,y,z,t) = E(r_t)\exp(j(\omega t + \beta (n \cdot r)))$$

where constant β is the propagation constant and invariant in the cross-section plane. We must note there is an unstated assumption that the propagating plane wave calculation

does not take the diffractive loss and radiative loss into account. These kind of loss mechanism may lead to the uneven loss in the waveguide cross-section.

We set the Al occupied domains as non-magnetic material with the modified permitivity from table 1, the other domains as air. The minimun mesh grid size is set less than 1/5 wavelength. The hybrid-mode wave equations which determine the field distribution with the satisfied boundary condition are bellow:

$$\begin{aligned} \nabla_t \times (\varepsilon_{rc}^{-1} \nabla_t \times h_t) - k_0^2 \mu_r h_t &= -\beta^2 \varepsilon_{rc}^{-1} (\nabla h_n / k_0 + h_t) \\ 0 &= \beta^2 \left(\frac{1}{k_0} \nabla_t \bullet \varepsilon_{rc}^{-1} (\nabla h_n / k_0 + h_t) + \mu_r h_n\right) \end{aligned} \tag{2}$$

where

$$h_t = \beta H_t, h_n = -jk_0 H_n, k_0 = 2\pi / \lambda \tag{3}$$

The COMSOL software solves the above equations by FEM mothod, given the boundary and subdomain conditions. Figure 6 shows the fundamental mode field distributions for different waveguide geometry and different frequencies. We define the fundamental mode is the mode as that without obivous cut-off frequency, and can dominantly couple the incoming Gaussian beam into the waveguide. We see that the electric field perpendicular to the metal plate has almost all of the waveguides energy, the characteristics of the called quasi-TEM mode.[20] The four conners of the Al plates have strong energy concentrations, which is due to the plasmonic edge effects. In this sense it is consistent with plasmonic slot waveguide simulations.[22] [21]

For small plate separation, the filed distribution tends to be more uniform inside the waveguide; also for the low frequency, the field distribution tends to be more uniform. In Fig 6 (a), the field distribution is like the traditional TEM mode distribution, except with a bit stronger four cornners. In Fig 6 (d), the field distribution is like the plasmonic mode, whose energy concentrated strongly in the four cornners. Fig 6(b) and (c) show the intermediate cases for the mode transition.

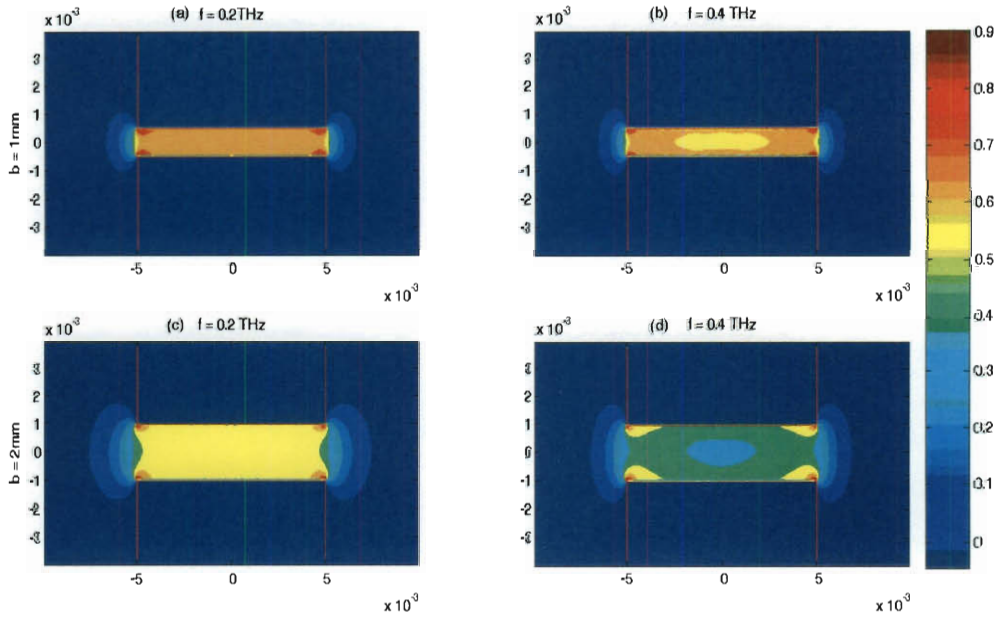

Figure 6 The 2D contour plots of perpendicular electric field strength for finite width PPWG. PPWG have cross-setion (a) (b) 1cm x 1mm. (c) (d) 1cm x 2mm. The frequency for (a) (c) is 0.2THz, for (b) (d) is 0.4 THz.

Corresponding to our experimental results we conduct a series of simulations for frequencies from 0.1THz to 0.5THz with 50GHz step, and for different plate separations. The same middle line scan analysis is applied to the simulation results in the same way as that in Fig4. Fig 7 shows the corresponding 2D color plot. We see the transition frequency shows the same behaviour as we obeserved in the experiment. It depends on the geometry of the waveguide and increases with the plate separation increasing.

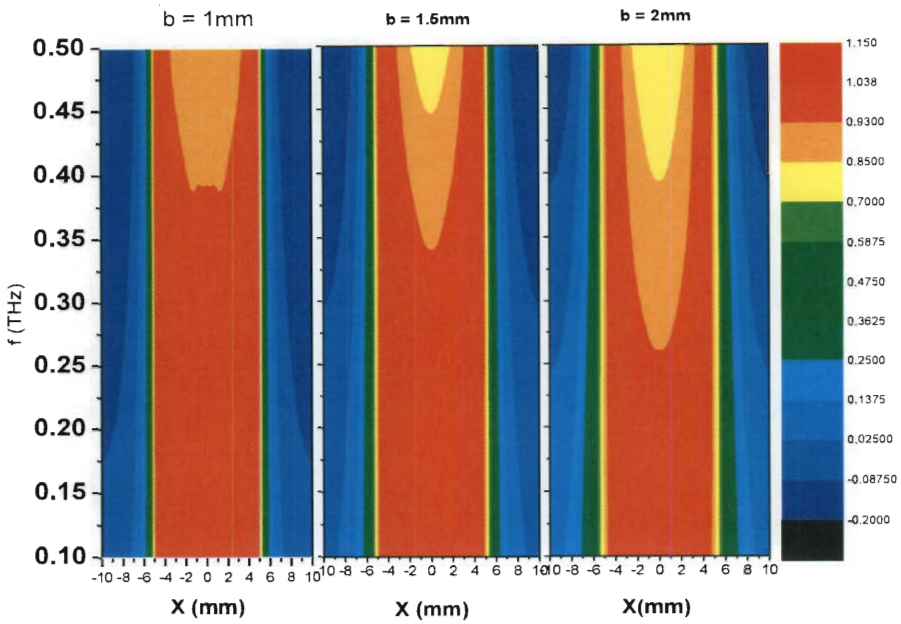

Figure 7 The simulated 2D electric filed contour plot for three plate spearations, 1mm, 1.5mm, 2mm. (from left to rigtht)

There is an obivous difference between simulation and the experiment, that is the simulated field distribution for quasi-TEM mode tends to be uniform across the waveguide, but it shows a single peak in the center of waveguide in the experiment. This is because the diffractive loss is not taken into account in the simulation. The assumption for waveguide the boundary analysis mode is the waveguide cross-section field pattern does not change due to propagation, and the propagation loss is applied to the cross-section as a whole (equation (1), (2)). So the diffraction is ignored in the simulation. This kind of mode analysis is a good approximation for closed waveguides, which the confine all the waves inside closed boundary, or for the waveguide with short propagation which suffer much less from diffractive loss, or for high frequency waves which has less diffraction. But in our finite-width PPWG, which is open waveguide, with the air

boundary on two sides and with propagation length ~22.5cm much longer than the wavelength, the diffractive loss should be taken into account. Since the diffraction is stronger for longer wavelength, so it should be stronger in low frequency (0.1 – 0.2 THz) than that in high frequency (0.3-0.5THz). Therefore considering these diffractive losses, we shoud expect filed distribution inside the waveguide shows single middle peak for low frequency, as we observed in the experiment.

All in all, collecting all the aspects above, we give a physical interpretation for our experiment. This finite width PPWG supports broad band THz waves from 0.05THz to 0.9 THz. For different plate separations and for different frequencies, the field distribution inside the waveguide is different. We can interpret the behavior of the waveguide mode as interaction between two surface waves supported by the two finite width metal plates. When the interaction between the two SP waves are strong, the waveguide shows quasi-TEM mode [23]When the two SP waves are more independent, the waveguide shows plasmonic mode, which has relatively strong edge effect [21]. The interaction between the two SP waves depends on plate separations and the wavelength. When the plate separation is small and the wavelength is long, the interaction is strong. When the two plates are far from each other and wavelength is short, they tends to support independent surface waves which shows strong edge effect. The independent THz surface waves on single plate is simulated in Figure 8.

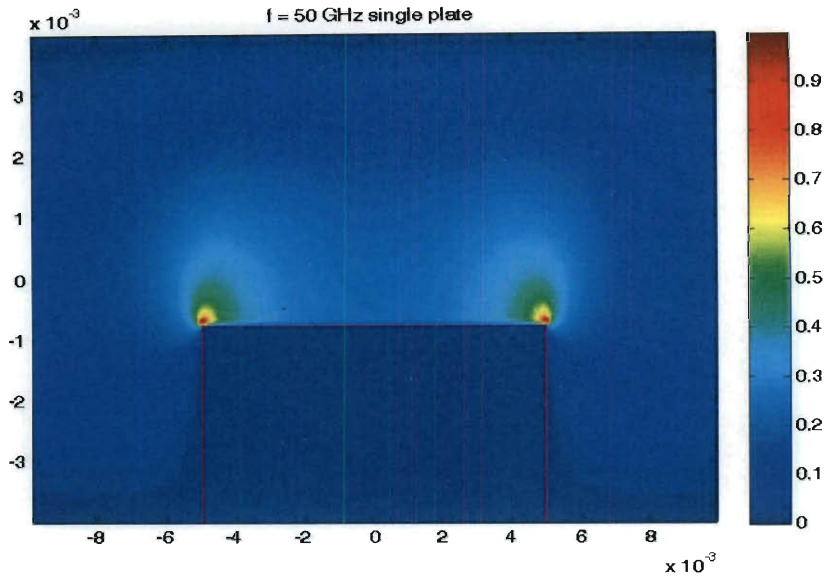

Figure 8 Independent THz surface waves on single Aluminum plate

We interpret the experiment from another view. We adopt a very simple model to calculate the independence of the two SP waves.We use the infinite-width PPWG shown in Figure 9 (a) to calculate the interaction of the supported two surface waves. For this simple case, we can get an accurate analytical description[23] [24] .

$$\psi(x) = \begin{cases} A\exp(-k_2(x-d)) & \cdots\cdots\cdots\cdots x > d \\ B\exp(k1(x-d)) + C\exp(-k1(x+d)) & \cdots\cdots |x| < d \\ D\exp(k2(x+d)) & \cdots\cdots\cdots\cdots x < -d \end{cases} \quad (4)$$

here

$$k_i = \pm\sqrt{r^2 - \omega^2\mu_0\varepsilon_i}$$

$$\frac{k_2\varepsilon_1}{k_1\varepsilon_2} = -\tanh(k_1 d)$$

where 1,2 correspond to air and aluminum plate respectively, k1 and k2 are the decay coefficient into the media, r is the propagation coefficient for the ' (5) uide, d is the plate separation. We must note that k1,k2 and r should be complex value. Given the permitivity of the air and aluminum (see table 1), we solve equation (5) numerically. With the solution of k1,k2, we get the field distribution of waveguide.

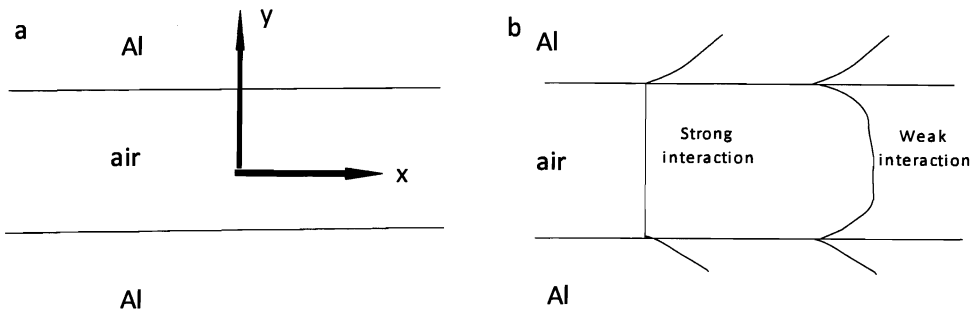

Figure 9 The scheme of the simple infinit-width PPWG model

The strong coupling of the two waves shows field distribution uniform across the air gap (quasi-TEM mode), while the weak coupling show stronger field close to metal plates and weaker in the middle of the air gap (plasmonic mode), Fig9 b. So we define the field delta ΔE as difference between the field on the metal plate and the field in the middle of the air gap. We use ΔE as an estimate of the independence of the two surface waves. The larger ΔE is, the stronger the independence is. By the analytical solution, we see ΔE depends on the plates separation and wavelength or frequency.

To define the mode transition frequency, we choose an arbitrary value ΔE_s ~ 5% as criteria to distrinct the strong interaction and weak interaction. For strong interaction, the waveguide is quasi-TEM mode and for weak interaction it is plasmonic

mode. By setting $\Delta E(f,b) = \Delta E\_s$, where f is frequency and b is the plate separation, we can solve the relationship between f and b shown in fig 5. The relation agrees with our experimental data with acceptible distinctions, which is expected since the plate width is different (infinite for calculation and 1cm for experiment).

5 . Conclusion

In summary, we have conducted the near-field measurement inside the THz finite width PPWG. In the THz range we find the waveguide mode transition from TEM-like mode to the plasmonic mode. And the mode transition depends on the geometry of the PPWG. This mode transition can be qualitatively attributed to the relatively large metal plasmonic response in higher frequency.

REFERENCES:

[1] R. Mendis and D. Grischkowsky, *Opt. Lett. 26, 846*, 2001.

[2] R. Mendis and D. Grischkowsky, *J. Appl. Phys. 88, 4449*, 2000.

[3] J.D. Jackson, *Classical Electrodynamics 3rd ed.* 1998.

[4] Adam Bingham, Yuguang Zhao, and D. Grischkowsky, *APPLIED PHYSICS LETTERS 87, 051101 (2005).*

[5] Z. Jian, J. Pearce and D. M. Mittleman, *Optics Letters, 29, 2067*, 2004.

[6] J.S. Melinger and D. Grischkowsky, *Guided Terahertz Waves for Characterizing Explosives,CHEMICAL/BIOCHEMICAL RESEARCH*, 2009.

[7] Michael Theuer, S. Sree Harsha, and D. Grischkowsky, *J. Appl. Phys. 108, 113105 2010.*

[8] S. Sree Harsha and D. Grischkowsky, *J. Phys. Chem. A, 2010, 114 (10), pp 3489–3494.*

[9] Joseph S. Melinger, S. Sree Harsha N. Laman, and D. Grischkowsky, *Vol. 26, No. 9,J. Opt. Soc. Am. B*, Sep. 2009.

[10] M. M. Awad and R. A. Cheville, *Appl. Phys. Lett. 86, 221107/1-3*, 2005.

[11] M. Nagel, P. H. Bolivar, and H. Kurz, *Semiconduct. Sci. Technol., vol. 20, pp. S281–S285*, 2005.

[12] R. Mendis, V. Astley, J. Liu, and D. M. Mittleman, *Applied Physics Letters, 95, 171113*, 2009.

[13] S. Sree Harsha, N. Laman, and D. Grischkowsky, *Appl. Phys. Lett. 94, 091118 2009*.

[14] H. Zhan, R. Mendis, and D. M. Mittleman, *Optics Express, 18, 9643-9650*, 2010.

[15] R. Yang, M. A. Abushagur, and Z. Lu, *Optics Express, Vol. 16, Issue 24, pp. 20142-20148*, 2008.

[16] E. R. Statz, K.-H. Lin, K. A. Nelson, M. Yang, and K. J. Webb, *Opt. Lett. 35, 2931-2933*, 2010.

[17] V. Astley, H. Zhan, R. Mendis, and D. M. Mittleman, *J. Appl. Phys. 105, 113117*, 2009.

[18] K. Wang, A. Barkan, and D. M. Mittleman, *Applied Physics Letters, 84, 305*, 2004.

[19] D. F. P. Pile, T. Ogawa, D. K. Gramotnev, Y. Matsuzaki, K. C. Vernon, K. Yamaguchi, T. Okamoto, M. Haraguchi, and M. Fukui, *Appl. Phys. Lett. 87(26), 261114*, 2005.

[20] T. Rozzi and M. Mongiardo, *Open electromagnetic waveguides*. 1999.

[21] G. Veronis and S. Fan, *Opt. Lett. 30, 3359–3361*, 2005.

[22] G. Veronis and S. Fan, *J. Lightwave Technol. 25, 2511-2521*, 2007.

[23] B. G. Ghamsari and A. H. Majedi, *J. Appl. Phys. 104, 083108*, 2008.

[24] B. G. Ghamsari and A. H. Majedi, *Proc. SPIE, Vol. 7311, 73110B*, 2009.

[25] H.M.Bralow and B.Sc(Eng.), C.Eng., F.I.E.E., F.R.S, *PROC. IEE, Vol. 114, No. R*, 1967.

[26] T. Jeon and D. Grischkowsky, *Appl. Phys. Lett. 88, 061113*, 2006.

[27] L.S. Mukina, M.M. Nazarov, A.P. Shkurinov, *Surface Science, Volume 600, Issue 20*, 2006.

[28] M. A. Ordal, L. L. Long, R. J. Bell, S. E. Bell, R. R. Bell, R. W. Alexander, Jr., and C. A. Ward, *Appl. Opt. Vol. 22, No. 7*, 1983.

[29] Smith, D. R., Pendry, J. B. & Wiltshire, M. C. K., *Science 305, 788–792*, 2004.

[30] García-Vidal, F.J., Martín-Moreno, L., and Pendry, J.B, *J. Opt. A: Pure Appl. Opt., 2005, 7, p. S97–S101*.